Corrugated Carbon Nanotube Microstructures with Geometrically Tunable Compliance

Michaël F. L. De Volder,[†,‡,§] Sameh Tawfick,[†] Sei Jin Park,[†] and A. John Hart[†,*]

[†]Department of Mechanical Engineering, University of Michigan, Ann Arbor, Michigan 48109, United States, [‡]Department of Mechanical Engineering, Katholieke Universiteit Leuven, 3001 Leuven, Belgium, and [§]IMEC, Kapeldreed 75, 3001 Heverlee, Belgium

ABSTRACT Deterministic organization of nanostructures into microscale geometries is essential for the development of materials with novel mechanical, optical, and surface properties. We demonstrate scalable fabrication of 3D corrugated carbon nanotube (CNT) microstructures, *via* an iterative sequence of vertically aligned CNT growth and capillary self-assembly. Vertical microbellows and tilted microcantilevers are created over large areas, and these structures can have thin walls with aspect ratios exceeding 100:1. We show these structures can be used as out-of-plane microsprings with compliance determined by the wall thickness and number of folds.

KEYWORDS: carbon nanotubes · three-dimensional · microstructure · spring · anisotropic · self-assembly

Folded and corrugated structures are a long-standing fascination spanning mathematics, physics, biology, and engineering. For example, the tunable structural compliance of folded bellows makes them widely used as mechanical springs, linear actuators, couplings, and moving seals; and re-entrant forms with high surface area are utilized in heat exchangers and filters. Re-entrant features are also essential to the performance of biomimetic actuators,[1] smart adhesives,[2] superhydrophobic,[3] self-cleaning,[4] and omniphobic,[5] surfaces. Further, materials having re-entrant internal topologies can exhibit novel mechanical properties including negative Poisson's ratio.[6−8] The ability to miniaturize folded and corrugated structures would thus be highly beneficial for the development of new microsystems, engineered surfaces, and metamaterials.

Nevertheless, it remains difficult to manufacture folded and re-entrant shapes in a scalable manner at small scales. Fabrication of re-entrant geometries often requires vertical structuring, which is typically done using multistep deposition and lithographic etching processes, or by rapid prototyping methods such as stereolithography,[9,10] multiphoton lithography,[11,12] and focused ion beam (FIB) processing.[13] While these latter approaches can create arbitrary forms, their serial nature is only practical for small production volumes. Additionally, lithographically patterned thin films have been folded out of plane by "micro-origami" methods, using residual stresses,[14,15] capillary forces,[16,17] or magnetic forces[18] to initiate folding. While these methods have demonstrated unique structures including vertical micromirrors and intricate closed polyhedra, stacking of sequentially folded microarchitectures has not been achieved.

Recently, many promising applications of vertically aligned carbon nanotube (CNT) "forests" have been demonstrated, including biomimetic adhesives,[19−23] elastic foams,[24] filtration membranes,[25] and thermal interfaces;[26] however, the geometries of CNT forests and patterned microstructures have been largely restricted to simple vertical and sloped shapes.[27] Nevertheless, we envision that an ability to make complex 3D microstructures out of CNTs, which are inspired by the geometry and applications of macroscale folded structures, could lead to further novel investigations. To this end, we present a method for high-throughput fabrication of corrugated three-dimensional (3D) CNT microstructures, enabling the engineering of novel multilevel architectures with both symmetric and asymmetric geometries. This method combines top-down lithographically patterned growth of carbon nanotubes (CNTs) with bottom-up locally directed elastocapillary self-assembly ("capillary forming").

RESULTS AND DISCUSSION

Figure 1A shows the iterative process by which hollow cylindrical CNT microstructures are formed into corrugated re-entrant shapes. The process begins by lithographic patterning of a catalyst film (1 nm Fe on 10 nm Al_2O_3, deposited by e-beam evaporation) on a silicon wafer, followed

* Address correspondence to ajohnh@umich.edu, michael.devolder@imec.be.

Received for review June 11, 2011 and accepted July 31, 2011.

Published online August 01, 2011
10.1021/nn202156q

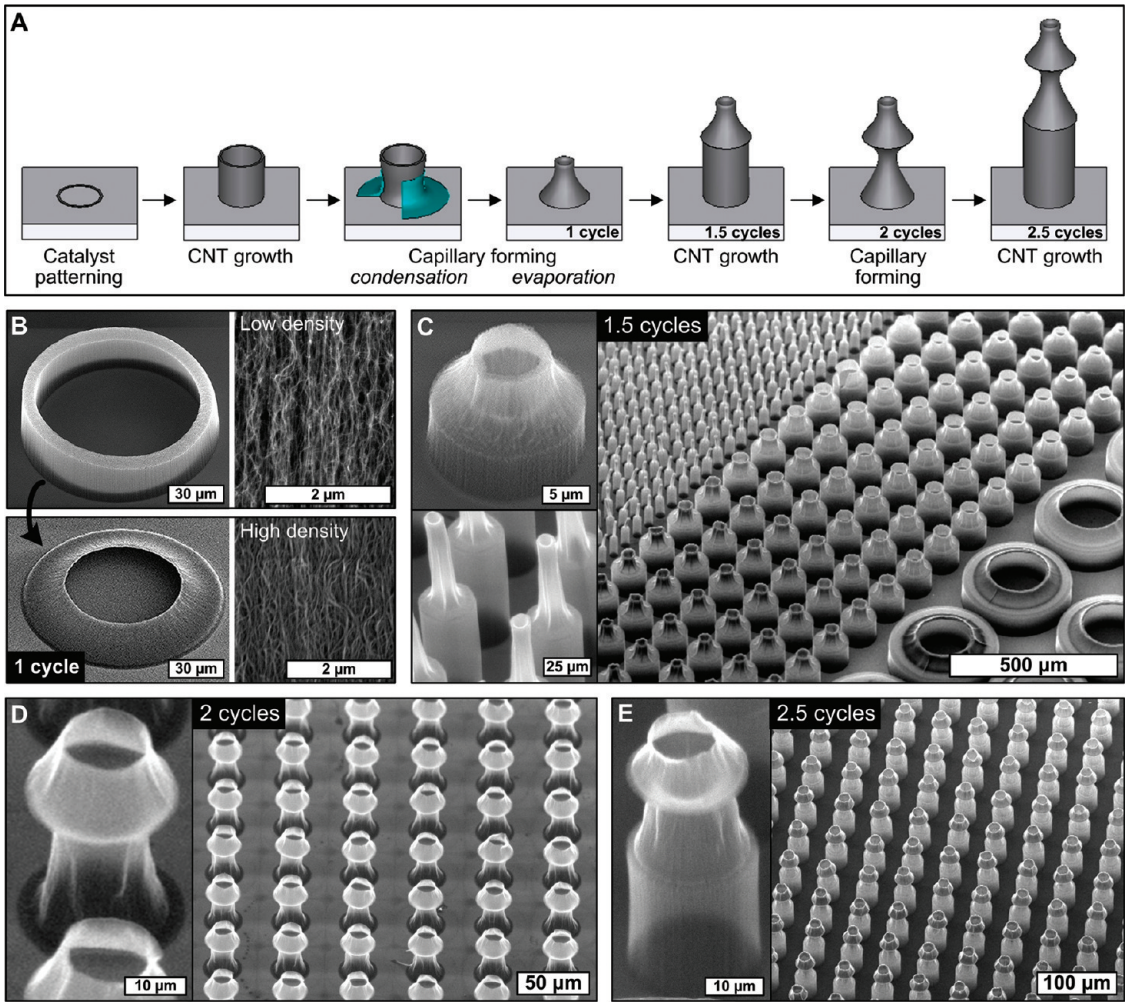

Figure 1. Fabrication of cylindrical CNT microbellows by iteration of growth and capillary forming: (A) schematic illustration of the iterative process; (B) SEM images of a cylindrical CNT microstructure before and after capillary forming (1 cycle), with close-up images emphasizing the densification of aligned CNTs; (C–E) SEM images of microstructures after consecutive growth, forming, and growth cycles, reaching 2.5 cycles in image E.

by growth of vertically aligned multiwall CNT "forest" microstructures by thermal CVD at atmospheric pressure (see Methods).[28] The CNT forest microstructures have straight walls, representing an "extrusion" of the catalyst pattern perpendicular to the substrate. Next, the straight CNT microstructures are transformed into sloped shapes by condensation and subsequent evaporation of liquid on the substrate. In this capillary forming step,[29] the self-directed capillary action of liquid in the aligned CNT network causes the CNTs to densify[30–34] by the well-known elastocapillary aggregation mechanism,[35–40] and the distribution of capillary forces throughout the microstructure results in an overall shape transformation.[29,41] For example, the hollow cylindrical CNT microstructures become sloped cones after capillary forming (Figure 1), and the slope angle is determined by the initial wall thickness of the cylinder, which adjusts the balance between capillary forces and structural deformation.

The combination of a single CVD growth and capillary forming operation, which we reported previously,[29] is the first cycle of the iterative process that is used to create corrugated structures. Iteration is possible because the CNT growth catalyst, which remains on the substrate at the base of the CNTs, can be reactivated[42,43] by simply repeating the CVD growth after capillary forming.

Therefore, the geometric attributes of the folded CNT structures are easily specified: the number of folds is controlled by the number of process cycles, and the height of each layer is determined by the corresponding CNT growth time. Starting with a short hollow cylinder of CNTs (first growth step), the first capillary forming step gives a sloped microwell (Figure 1B);[29] the second growth step lifts the well from the substrate (Figure 1C); the second capillary forming step shapes the newly grown portion (Figure 1D), without changing the shape of the upper portion made during the first cycle; and the third growth step lifts the structures made during the first two cycles (Figure 1E). Because liquid is confined within each structure during capillary forming, arrays of structures with greatly different lateral dimensions (*i.e.*, from <10 μm to >100 μm,

as in Figure 1C) can be fabricated in close proximity on the same substrate, thus enabling integration of heterogeneous architectures in a scalable way. All the structures are defined by the single photolithography step that patterns the catalyst islands; therefore no secondary alignment or lithography steps are needed.

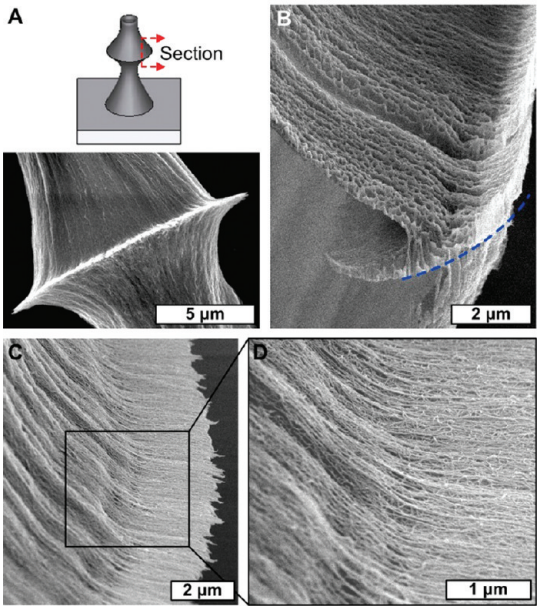

Figure 2. Analysis of the interlayer between sections of a corrugated CNT structure: (A) schematic of section location, and image of pristine joint; (B) FIB cross-section, revealing the interface between the CNTs that are drawn to the substrate during capillary formation (above the dashed arc), and the CNTs produced by the subsequent growth step (below the line); (C,D) transition of aligned CNTs from the sloped sidewall to the interface.

Notably, capillary forming of a newly grown (bottom) section does not disturb the geometry of the previously made (upper) section. When this newly grown portion is capillary formed, it takes a concave shape (Figures 1D and 2A), indicating that it is constrained rigidly on both its top and bottom surfaces. This constraint is provided by a stiff layer formed at the interface between sections of the corrugated structures (Figure 2A), which enables the formation of subsequent re-entrant structures. The interlayer forms because the CNTs at the base of the structure are pulled down to the substrate by the surface tension of the liquid during capillary forming. The stiffness of the interlayer is enhanced by the self-organization of CNTs during the following growth step, representing the tangled "crust" which is typically observed at the top of CNT forests.[44,45] We examined the internal structure of this interface by taking a focused ion beam (FIB) cross-section (Figure 2B), and note the CNTs transition smoothly from the sloped section to the flat interlayer (Figure 2C,D).

After observing this interlayer, we sought to learn if similar re-entrant shapes could be fabricated using a single CVD step with pulsed gas flows, and a single capillary-forming step after the CVD process. Our idea was to interrupt CNT growth by stopping the hydrocarbon (C_2H_4) flow, and to repeat this interrupted sequence for the desired number of cycles. As shown in Figure 3, this alternative approach does not lead to the re-entrant circular shapes, because the stiff interlayer is not created. For example, interrupting the C_2H_4 flow while keeping the temperature constant gives horizontal "stripes" on the CNT structures (Figure 3A),

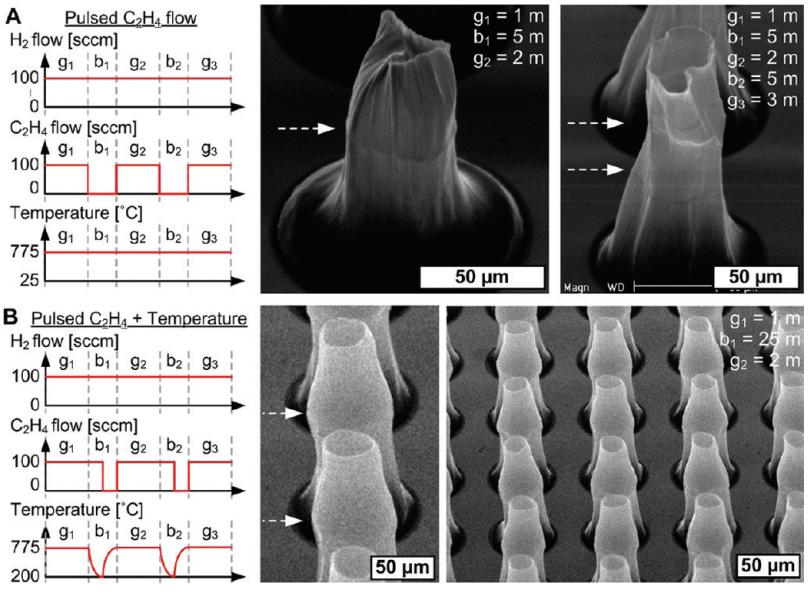

Figure 3. Investigation of pulsed gas and temperature sequences for the fabrication of corrugated microstructures, where one capillary forming operation was performed after the complete sequence: (A) pulsing of hydrocarbon source only, resulting in "striped" microstructures that densify uniformly without re-entrant shapes; (B) pulsing of both hydrocarbon source and temperature, resulting in slight re-entrant curvature.

but the structures densify uniformly from bottom to top. Interrupting the C_2H_4 flow and cycling the furnace temperature results in slight re-entrant curvature (Figure 3B), indicating that the structure of the forest is modified at the location of the interruption, but this segment also contracts inward upon densification. In contrast, when CVD and capillary forming steps are alternated as discussed previously, the perimeter of the stiff interface between the segments does not densify and remains the same as the initial catalyst shape (Figure 1). In the preferred method, the CNTs at the base of the newly grown segment are pulled downward to the substrate during each capillary forming step. Therefore, the stiff interlayer that pins the re-entrant shapes forms due to the interaction between the bottom of the CNT structure and the substrate during capillary forming, and the self-organization of CNTs at the beginning of each growth step.

Next, we investigated the utility of the cylindrical CNT "bellows" shown in Figure 1 for use as vertical microsprings. Microspring arrays are used commercially in probecards for the testing of electronic devices.[46,47] The need for arrays of compliant springs with a small footprint has stimulated the development of complicated multistep electrodeposition and wire-bonding processes for fabrication of overhanging microcantilevers.[47] We found that the properties of the corrugated CNT microsprings can be tuned on the basis of their geometry alone, and their vertically compliant design gives these springs a small footprint.

Figure 4A shows an exemplary array of vertically structured springs, where the wall thickness increases from left to right across the array. The height of each segment is shown in Figure 4B. The stiffness of each spring was measured using a nanoindentation tool (MTS Nano Indenter XP), by compressing the spring using a spherical tip that was aligned to the center of the spring. Use of a large tip with 250 μm diameter ensured measurement of the collective elastic properties of each microspring rather than the local (nanoscale) properties. Two arrays of springs were tested: one with a single fold (2 cycles, similar to Figure 1E); and one with two folds (3.5 cycles, as shown in Figure 4). After growth and forming, the springs were coated with 200 nm of Parylene-C. This coating step approximately doubled the stiffness of the structures, and significantly increased their elastic range. In total, approximately 50 springs were individually compressed three times each. Typical load-unload curves for springs with different wall thicknesses are shown in Figure 4C.

The compliance (reciprocal of the stiffness) of the springs is inversely related to the wall thickness, as shown in Figure 4D. This relationship is understood by modeling the mechanical behavior of the microbellows. We observed that the geometry of the structures is analogous to a series of conical disk springs (aka "Belleville washers") used in mechanical systems, and

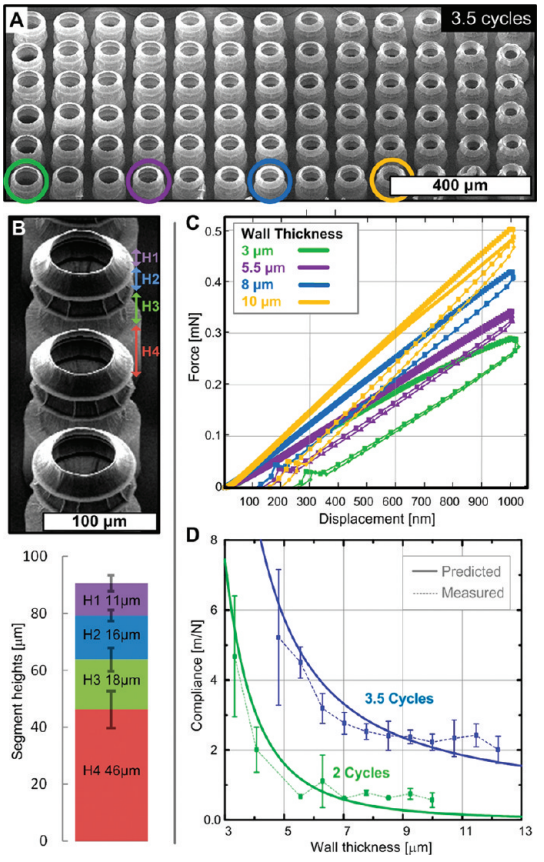

Figure 4. Tunable compliance of corrugated CNT microsprings: (A) array of springs with wall thickness increasing from left to right, processed for 3.5 cycles; (B) row of springs with identical wall thickness, and height measurements of the subsequent regrowth segments; (C) load−displacement curves for parylene-coated microsprings with a wall thickness of 3−10 μm; (D) measured and predicted compliance of individual parylene-coated springs *versus* wall thickness.

we found that the compliance of the CNT microbellows can be predicted using conventional disk spring equations.[48,49] Thus, the compliance (S) of a microspring is

$$S = \frac{n{d_o}^2}{4kE_d s^3} + \frac{L}{E_u A} \quad (1)$$

In the first term of this equation, n is the number of processing cycles, d_o is the outer diameter of the bellows, k is a geometry factor for conical shells (here 1.5), E_d is the elastic modulus of the capillary formed CNT wall, and s is the wall thickness. The second term of eq 1 applies to the structures made with 3.5 cycles and represents the compliance of the bottom section which was not densified. The compliance of this section is proportional to its height L, and inversely proportional to the product of the elastic modulus of the undensified CNT forest (E_u) and the area of the cylinder A.

As seen in Figure 4D, the predicted and measured values show similar trends, confirming that the compliance is inversely proportional to s^3. The compliance

is tuned 20-fold by varying the wall thickness by catalyst patterning, and varying the number of corrugations, while keeping the outside diameter of the spring constant. Therefore, wide-range and local control of the mechanical properties of the microsprings is enabled solely by choice of the processing parameters.

The properties of the corrugated CNT microstructures presented here can be compared to CNT forests known as supercompressible CNT foams.[24] The previous foams are nonpatterned CNT forests comprising large-diameter multiwall CNTs with a relatively high as-grown packing density. The reported average mechanical stiffness of CNT foams is 26 kPa/μm, giving an elastic modulus of $E = 50$ MPa for a bulk pore density of 87%. The corrugated bellows fabricated in this study can be considered as building blocks for microporous CNT foams while permitting 3D control of the foam topology along with the elastic properties. In the CNT bellows, the elastic modulus of the densified CNT wall is 4 GPa, and the stiffness is tuned from 25.5 to 127.5 kPa/μm by changing the wall thickness s and the number of cycles. This, in turn, varies the microporosity (the portion of empty volume within the bellow) from 87% to 94%. While the previous supercompressible CNT forests can withstand at least 20% of fully elastic strain, the bellows structures shown in Figure 4 crack and exhibit plastic deformation at strokes leading to strains larger than 5%. Nevertheless, the springs shown here recover fully upon compression of up to ~5 μm (depending on wall thickness), and the reported compliance is for the fully elastic range.

Additional compression tests were performed to investigate the failure mode of the CNT microsprings. As shown in Figure 5, arrays of uncoated springs (2 cycles) were intentionally compressed far beyond the elastic regime. As seen in the close-up images, the walls of the springs either buckle or tear. Cracks propagate in a direction locally parallel to the CNTs. This behavior is corroborated by the force-displacement curves (D), showing that the pillars do not recover elastically. The observed failure modes may be exacerbated by local variations in CNT density or by misalignment of the spherical compression tip, causing local stress concentrations. We envision that coating the CNTs with thin layers of polymer or ceramic (*e.g.*, by CVD or ALD) procedure could greatly enhance the robustness of the springs by reinforcing the lateral interaction among the CNTs. Investigation of the fatigue life of the springs, within the elastic range, will also be necessary.

In addition to axisymmetric bellows, anisotropic corrugated structures can be made starting from asymmetric catalyst patterns, as shown in Figure 6A. We previously found that capillary forming of semicylindrical CNT micropillars causes the pillars to deterministically bend during densification, toward the curved side of the semicircular cross section (Figure 6B).[29,41] Now, we show that iteration of growth and forming of

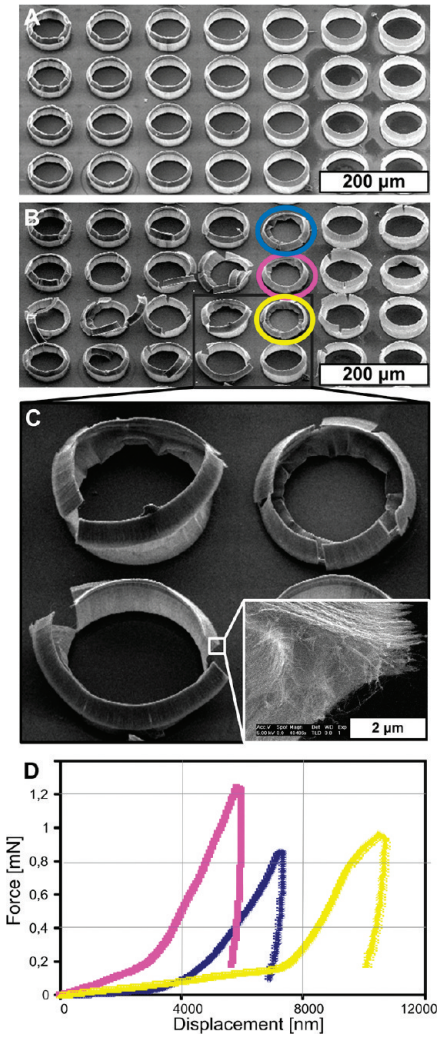

Figure 5. Failure modes of corrugated CNT microsprings: (A) array of cylindrical microsprings (2 cycles) before indentation; (B) same array after compression with large (>5 μm) stroke; (c) close up of microsprings after compression, showing cracked and buckled areas; (d) force-displacement curves of springs highlighted in panels B and C.

semicircular shapes creates intricate overhanging cantilevers with multiple folds (Figure 6C–F). The structures can be packed in dense arrays and oriented in any direction (*e.g.*, Figure 6E). We anticipate that these slanted structures will be particularly useful in design of surfaces with anisotropic wetting properties[50] and directional adhesives;[2,51] where the asymmetric geometry, nanoscale texture, mechanical compliance, and strong van der Waals attraction of the CNTs could be advantageous.

Additional structures shown in Figure 7 highlight the current dimensional limitations of the corrugation technique. First, as shown in Figure 7A, tall structures that have been processed for many cycles can become fragile and fall over, or are aggregated by capillary forces. At these limits, the robustness of the structures is limited by the decay of CNT density that occurs as the total growth duration (number of cycles) increases.[52] The CNT growth rate also decreases with each cycle, as

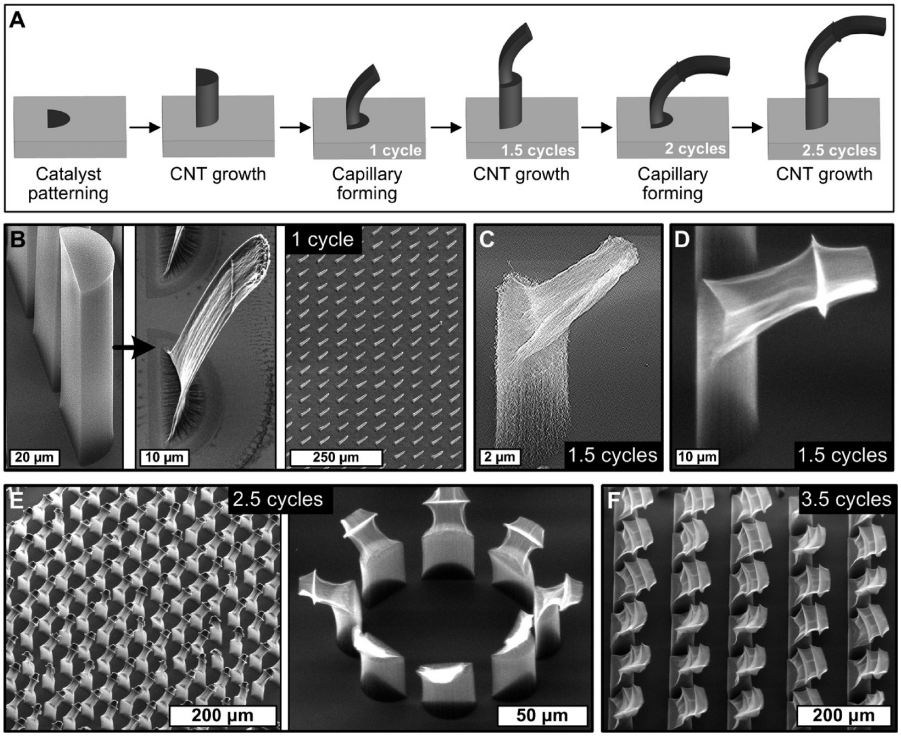

Figure 6. Fabrication of corrugated CNT cantilevers by the iterative growth-forming process: (A) schematic of process sequence; (B) individual cantilevers after consecutive processing cycles; (C) unidirectional and multidirectional arrays, processed for 2.5 and 3.5 cycles.

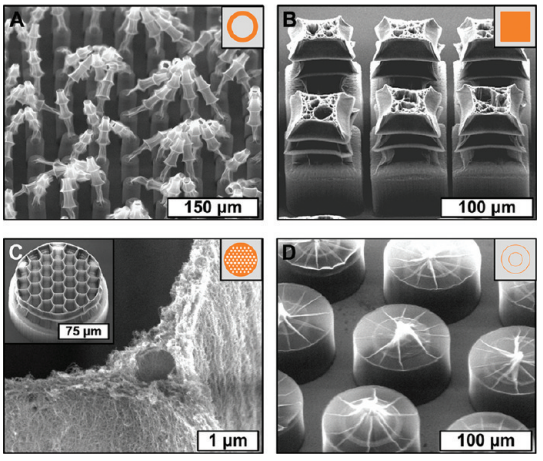

Figure 7. Dimensional limits of the corrugation process: (A) aggregation of hollow, tall, closely spaced structures after 3.5 cycles; (B) solid square patterns that form internal voids due to elastocapillary aggregation (3.5 cycles); (C) large-area micropillar with honeycomb core made by prepatterning array of holes within the pillar (2.5 cycles); (D) cylindrical microcontainers created by capillary folding of thin CNT sheets followed by a second growth step (1.5 cycles).

a longer time is needed to produce consecutive segments of equal height. Another limitation is shown in Figure 7B, where relatively large-area pillars exhibit internal voids due to elastocapillary aggregation of CNTs, unlike the smaller structures that densify into a void-free structure.[40] Formation of voids can be controlled by prepatterning holes within the area of the CNT forest, as shown in Figure 7C. In both cases of void formation, the corrugated topology can still be made by iterative processing. In the latter case, the prepatterned voids transform into a reinforcing honeycomb core upon capillary forming, and the walls of the honeycomb shown are less than 300 nm thick. The aspect ratio (height/thickness) of the honeycomb walls, as well as the conical shells of the bellows shown earlier (Figure 2B), can exceed 100:1. This is beyond the typical capabilities of microfabrication thin vertical structures, including use of X-ray lithography to pattern high-aspect-ratio polymer features at sub-micrometer scale.[53] Finally, intricate closed microcontainers (Figure 7D) are fabricated by capillary forming of short hollow concentric CNT cylinders, which fold inward during capillary forming, and are lifted up from the substrate in the second growth step.

CONCLUSION

We presented a new 3D structuring method for vertically aligned nanostructures, *via* an iterative sequence of CVD growth of CNTs and elastocapillary self-assembly. We fabricated a wide variety of 3D CNT microstructures, including circular bellow springs with controllable compliance, arrays of anisotropic and multidirectional features. We envision that our approach to create novel corrugated structures can be applied to the fabrication of many other nanostructure geometries and can be combined with known methods to engineer the diameter and packing density of CNTs (*i.e.*, for single-wall[42] or multiwall[54–56] forests) as

well as many types of nanowires. By calibrating the time-dependent growth rate of the CNTs and by automating the growth and forming sequence, highly intricate structures with tens of corrugations should be possible. Corrugated spring designs that combine micromechanics with the collective elastic properties of aligned CNTs may offer further tunability, including management of both energy storage and dissipation, and engineering of mechanical instabilities.[57,58] Further attractive properties of CNTs suggest it will be possible to create 3D microstructures that offer novel multifunctionality, such as coupling between mechanical deformation and electrical conductivity, and combinations of corrugated topographies with chemical and biochemical surface functionalities.

METHODS

CNT Growth. CNT forest microstructures are fabricated on thermally oxidized (100) silicon wafers on which 10 nm of Al_2O_3 and 1 nm Fe are sequentially deposited by e-beam evaporation. The catalyst is patterned by liftoff using photoresist SPR 220 and ultrasonic agitation in acetone followed by an isopropyl alcohol rinse. Next, CNT forests are grown in a horizontal tube furnace (22 mm ID, 300 mm heated length) at atmospheric pressure, with flows of 100/400/100 sccm C_2H_4/H_2/He, at 775 °C. The CNTs are rapidly cooled in the growth atmosphere before purging the CVD chamber with He. This is done by opening the tube furnace once the desired growth time is achieved. Typical growth times for the structures shown in this paper are 0.5 min for the first cyle; 1 min for the second cycle; 1.5 min for the third cycle; and 2 min for the last growth.

Capillary Forming. First, a small amount of acetone (~20 mL) is heated in a large beaker (1 L) on a hot plate. Once the acetone is boiling, the Si substrate containing the CNT structures is attached to an aluminum mesh and is inverted over the beaker. The lower temperature of the Si substrate drives the condensation of the acetone, which in turn causes the CNTs to densify by capillary action. A more complete description of this process and its geometric limits has been published separately together with a detailed description of the experimental setup.[40]

Compression Testing. The stiffness of the corrugated microsprings was measured using a nanoindentation tool (MTS Nano Indenter XP) with a 250 micrometer-spherical tip. First, the tip is aligned to the bellow using a microscope. Each spring was indented three times, and three different springs with the same dimensions were tested. Indentations ranging from 1 to 6 μm were performed.

Acknowledgment. We thank K. Vanstreels for help with microcompression testing. This work was supported by the Fund for Scientific Research Flanders (FWO) Belgium, the Nanomanufacturing Program of the National Science Foundation (CMMI-0927364). Microfabrication was performed at the Michigan Lurie Nanofabrication Facility (LNF) and IMEC. Electron microscopy was performed at the Michigan Electron Microbeam Analysis Laboratory (EMAL) and IMEC.

REFERENCES AND NOTES

1. Brackenbury, J. Fast Locomotion in Caterpillars. *J. Insect Physiol.* **1999**, *45*, 525–533.
2. Gao, H. J.; Wang, X.; Yao, H. M.; Gorb, S.; Arzt, E. Mechanics of Hierarchical Adhesion Structures of Geckos. *Mech. Mater.* **2005**, *37*, 275–285.
3. Gao, X. F.; Jiang, L. Water-Repellent Legs of Water Striders. *Nature* **2004**, *432*, 36.
4. Blossey, R. Self-Cleaning Surfaces—Virtual Realities. *Nat. Mater.* **2003**, *2*, 301–306.
5. Tuteja, A.; Choi, W.; Mabry, J. M.; McKinley, G. H.; Cohen, R. E. Robust Omniphobic Surfaces. *Proc. Natl. Acad. Sci. U. S. A.* **2008**, *105*, 18200–18205.
6. Lakes, R. Foam Structures with a Negative Poissons Ratio. *Science* **1987**, *235*, 1038–1040.
7. Evans, K. E.; Alderson, A. Auxetic Materials: Functional Materials and Structures From Lateral Thinking!. *Adv. Mater.* **2000**, *12*, 617–628.
8. Bertoldi, K.; Reis, P. M.; Willshaw, S.; Mullin, T. Negative Poisson's Ratio Behavior Induced by an Elastic Instability. *Adv. Mater.* **2010**, *22*, 361–366.
9. Bertsch, A.; Jiguet, S.; Renaud, P. Microfabrication of Ceramic Components by Microstereolithography. *J Micromech. Microeng.* **2004**, *14*, 197–203.
10. Stampfl, J.; Baudis, S.; Heller, C.; Liska, R.; Neumeister, A.; Kling, R.; Ostendorf, A.; Spitzbart, M. Photopolymers with Tunable Mechanical Properties Processed by Laser-Based High-Resolution Stereolithography. *J. Micromech. Microeng.* **2008**, *18*, 125014.
11. LaFratta, C. N.; Fourkas, J. T.; Baldacchini, T.; Farrer, R. A. Multiphoton Fabrication. *Angew. Chem., Int. Ed.* **2007**, *46*, 6238–6258.
12. Kawata, S.; Sun, H. B.; Tanaka, T.; Takada, K. Finer Features for Functional Microdevices—Micromachines Can be Created with Higher Resolution Using Two-Photon Absorption. *Nature* **2001**, *412*, 697–698.
13. Reyntjens, S.; Puers, R. A Review of Focused Ion Beam Applications in Microsystem Technology. *J. Micromech. Microeng.* **2001**, *11*, 287–300.
14. Arora, W. J.; Nichol, A. J.; Smith, H. I.; Barbastathis, G. Membrane Folding to Achieve Three-Dimensional Nanostructures: Nanopatterned Silicon Nitride Folded with Stressed Chromium Hinges. *Appl. Phys. Lett.* **2006**, *88*, 053108.
15. Leong, T. G.; Benson, B. R.; Call, E. K.; Gracias, D. H. Thin Film Stress Driven Self-Folding of Microstructured Containers. *Small* **2008**, *4*, 1605–1609.
16. Leong, T. G.; Lester, P. A.; Koh, T. L.; Call, E. K.; Gracias, D. H. Surface Tension-Driven Self-Folding Polyhedra. *Langmuir* **2007**, *23*, 8747–8751.
17. Guo, X.; Li, H.; Yeop Ahn, B.; Duoss, E. B.; Hsia, K. J.; Lewis, J. A.; Nuzzo, R. G. Two- and Three-Dimensional Folding of Thin Film Single-Crystalline Silicon for Photovoltaic Power Applications. *Proc. Natl. Acad. Sci. U. S. A.* **2009**, *106*, 20149–20154.
18. In, H. J.; Lee, H.; Nichol, A. J.; Kim, S.-G.; Barbastathis, G. Carbon Nanotube-Based Magnetic Actuation of Origami Membranes. *Proc. Am. Vac. Soc.* **2008**, 2509–2512.
19. Hill, F. A.; Havel , T. F.; Hart, A. J.; Livermore, C. Characterizing The Failure Processes that Limit the Storage of Energy in Carbon Nanotube Springs Under Tension. *J. Micromech. Microeng.* **2010**, *20*, 104012.
20. Jeong, H. E.; Suh, K. Y. Nanohairs and Nanotubes: Efficient Structural Elements for Gecko-Inspired Artificial Dry Adhesives. *Nano Today* **2009**, *4*, 335–346.
21. Ge, L.; Sethi, S.; Ci, L.; Ajayan, P. M.; Dhinojwala, A. Carbon Nanotube-Based Synthetic Gecko Tapes. *Proc. Natl. Acad. Sci. U. S. A.* **2007**, *104*, 10792–10795.
22. Kordas, K.; Toth, G.; Moilanen, P.; Kumpumaki, M.; Vahakangas, J.; Uusimaki, A.; Vajtai, R.; Ajayan, P. M. Chip Cooling with Integrated Carbon Nanotube Microfin Architectures. *Appl. Phys. Lett.* **2007**, *90*, 123105.
23. Baughman, R. H.; Zakhidov, A. A.; de Heer, W. A. Carbon Nanotubes—The Route toward Applications. *Science* **2002**, *297*, 787–792.

24. Cao, A.; Dickrell, P. L.; Sawyer, W. G.; Ghasemi-Nejhad, M. N.; Ajayan, P. M. Super-Compressible Foamlike Carbon Nanotube Films. *Science* **2005**, *310*, 1307–1310.
25. Holt, J. K.; Park, H. G.; Wang, Y. M.; Stadermann, M.; Artyukhin, A. B.; Grigoropoulos, C. P.; Noy, A.; Bakajin, O. Fast Mass Transport through Sub-2-Nanometer Carbon Nanotubes. *Science* **2006**, *312*, 1034–1037.
26. Tong, T.; Zhao, Y.; Delzeit, L.; Kashani, A.; Meyyappan, M.; Majumdar, A. Dense, Vertically Aligned Multiwalled Carbon Nanotube Arrays as Thermal Interface Materials. *IEEE Trans. Compon., Packag. Technol.* **2007**, *30*, 92–100.
27. De Volder, M.; Tawfick, S.; Hart, A. J. Controlled Growth Orientation of Carbon Nanotube Pillars by Catalyst Patterning in Microtrenches. *Proc. Transducers* **2009**, 2046–2049.
28. Hart, A. J.; Slocum, A. H. Rapid Growth and Flow-Mediated Nucleation of Millimeter-Scale Aligned Carbon Nanotube Structures from a Thin-Film Catalyst. *J. Phys. Chem. B* **2006**, *110*, 8250–8257.
29. De Volder, M.; Tawfick, S. H.; Park, S. J.; Copic, D.; Zhao, Z. Z.; Lu, W.; Hart, A. J. Diverse 3D Microarchitectures Made by Capillary Forming of Carbon Nanotubes. *Adv. Mater.* **2010**, *22*, 4384–4389.
30. Chakrapani, N.; Wei, B. Q.; Carrillo, A.; Ajayan, P. M.; Kane, R. S. Capillarity-Driven Assembly of Two-Dimensional Cellular Carbon Nanotube Foams. *Proc. Natl. Acad. Sci. U. S. A.* **2004**, *101*, 4009–4012.
31. Liu, H.; Li, S. H.; Zhai, J.; Li, H. J.; Zheng, Q. S.; Jiang, L.; Zhu, D. B. Self-Assembly of Large-Scale Micropatterns on Aligned Carbon Nanotube Films. *Angew. Chem. Int. Ed.* **2004**, *43*, 1146–1149.
32. Futaba, D. N.; Miyake, K.; Murata, K.; Hayamizu, Y.; Yamada, T.; Sasaki, S.; Yumura, M.; Hata, K. Dual Porosity Single-Walled Carbon Nanotube Material. *Nano Lett.* **2009**, *9*, 3302–3307.
33. Liu, Z.; Bajwa, N.; Ci, L.; Lee, S. H.; Kar, S.; Ajayan, P. M.; Lu, J. Q. Densification of Carbon Nanotube Bundles for Interconnect Application. *Proc. IEEE Electron Devices Soc.* **2007**, 201–203.
34. Futaba, D. N.; Hata, K.; Yamada, T.; Hiraoka, T.; Hayamizu, Y.; Kakudate, Y.; Tanaike, O.; Hatori, H.; Yumura, M.; Iijima, S. Shape-Engineerable and Highly Densely Packed Single-Walled Carbon Nanotubes and Their Application as Super-Capacitor Electrodes. *Nat. Mater.* **2006**, *5*, 987–994.
35. Roman, B.; Bico, J. Elasto-Capillarity: Deforming an Elastic Structure with a Liquid Droplet. *J. Phys. Condens. Mater.* **2010**, *22*, 493101.
36. Py, C.; Bastien, R.; Bico, J.; Roman, B.; Boudaoud, A. 3D Aggregation of Wet Fibers. *Europhys. Lett.* **2007**, *77*, 44005.
37. Bico, J.; Roman, B.; Moulin, L.; Boudaoud, A. Elastocapillary Coalescence in Wet Hair. *Nature* **2004**, *432*, 690–690.
38. Pokroy, B.; Kang, S. H.; Mahadevan, L.; Aizenberg, J. Self-Organization of a Mesoscale Bristle into Ordered, Hierarchical Helical Assemblies. *Science* **2009**, *323*, 237–240.
39. Tawfick, S.; De Volder, M.; Hart, A. J. Structurally Programmed Capillary Folding of Carbon Nanotube Assemblies. *Langmuir* **2011**, *27*, 6389–6394.
40. De Volder, M. F. L.; Park, S. J.; Tawfick, S. H.; Vidaud, D. O.; Hart, A. J. Fabrication and Electrical Integration of Robust Carbon Nanotube Micropillars by Self-Directed Elastocapillary Densification. *J. Micromech. Microeng.* **2011**, *21*, 045033.
41. Zhao, Z.; Tawfick, S. H.; Park, S. J.; De Volder, M.; Hart, A. J.; Lu, W. Bending of Nanoscale Filament Assemblies by Elastocapillary Densification. *Phys. Rev. E* **2010**, *82*, 041605.
42. Hata, K.; Futaba, D. N.; Mizuno, K.; Namai, T.; Yumura, M.; Iijima, S. Water-Assisted Highly Efficient Synthesis of Impurity-free Single-Walled Carbon Nanotubes. *Science* **2004**, *306*, 1362–1364.
43. Pint, C. L.; Nicholas, N.; Duque, J. G.; Parra-Vasquez, A. N. G.; Pasquali, M.; Hauge, R. Recycling Ultrathin Catalyst Layers for Multiple Single-Walled Carbon Nanotube Array Regrowth Cycles and Selectivity in Catalyst Activation. *Chem. Mater.* **2009**, *21*, 1550–1556.
44. Zhang, L.; Li, Z. R.; Tan, Y. Q.; Lolli, G.; Sakulchaicharoen, N.; Requejo, F. G.; Mun, B. S.; Resasco, D. E. Influence of a Top Crust of Entangled Nanotubes on the Structure of Vertically Aligned Forests of Single-Walled Carbon Nanotubes. *Chem. Mater.* **2006**, *18*, 5624–5629.
45. De Volder, M. F. L.; Vidaud, D. O.; Meshot, E. R.; Tawfick, S.; Hart, A. J. Self-Similar Organization of Arrays of Individual Carbon Nanotubes and Carbon Nanotube Micropillars. *Microelectron. Eng.* **2010**, *87*, 1233–1238.
46. Pruitt, B. L.; Park, W. T.; Kenny, T. W. Measurement System for Low Force and Small Displacement Contacts. *J. Microelectromech. Syst.* **2004**, *13*, 220–229.
47. Novitsky, J.; Miller, C. Wafer-Level CSP, Wafer-Level Assembly/Test: Integrating Backend Processes. *Solid State Technol.* **2001**, *44*, 78–80.
48. Almen, J. O.; Laszlo, A. The Uniform-Section Disk Spring. *Trans. ASME* **1936**, *58*, 305–314.
49. M. Hermann, A. J. *Static Characteristics of Flexible Bellows*. Master's Degree Thesis, University of Karlskrona, Sweden, **1997**.
50. Malvadkar, N. A.; Hancock, M. J.; Sekeroglu, K.; Dressick, W. J.; Demirel, M. C. An Engineered Anisotropic Nanofilm with Unidirectional Wetting Properties. *Nat. Mater.* **2010**, *9*, 1023–1028.
51. Boesel, L. F.; Greiner, C.; Arzt, E.; del Campo, A. Gecko-Inspired Surfaces: A Path to Strong and Reversible Dry Adhesives. *Adv. Mater.* **2010**, *22*, 2125–2137.
52. Bedewy, M.; Meshot, E. R.; Guo, H. C.; Verploegen, E. A.; Lu, W.; Hart, A. J. Collective Mechanism for the Evolution and Self-Termination of Vertically Aligned Carbon Nanotube Growth. *J. Phys. Chem. C* **2009**, *113*, 20576–20582.
53. Bogdanov, A. L.; Peredkov, S. S. Use Of Su-8 Photoresist for Very High Aspect Ratio X-ray Lithography. *Microelectron. Eng.* **2000**, *53*, 493–496.
54. Yamada, T.; Namai, T.; Hata, K.; Futaba, D. N.; Mizuno, K.; Fan, J.; Yudasaka, M.; Yumura, M.; Iijima, S. Size-Selective Growth of Double-Walled Carbon Nanotube Forests from Engineered Iron Catalysts. *Nat. Nanotechnol.* **2006**, *1*, 131–136.
55. Meshot, E. R.; Plata, D. L.; Tawfick, S.; Zhang, Y. Y.; Verploegen, E. A.; Hart, A. J. Engineering Vertically Aligned Carbon Nanotube Growth by Decoupled Thermal Treatment of Precursor and Catalyst. *ACS Nano* **2009**, *3*, 2477–2486.
56. Zhang, Y.; Gregoire, J.; Van Dover, R.; Hart, A. Ethanol-Promoted High-Yield Growth of Few-Walled Carbon Nanotubes. *J. Phys. Chem. C* **2010**, *114*, 6389–6395.
57. Suhr, J.; Victor, P.; Sreekala, L. C. S.; Zhang, X.; Nalamasu, O.; Ajayan, P. M. Fatigue Resistance of Aligned Carbon Nanotube Arrays under Cyclic Compression. *Nat. Nanotechnol.* **2007**, *2*, 417–421.
58. Cao, A. Y.; Dickrell, P. L.; Sawyer, W. G.; Ghasemi-Nejhad, M. N.; Ajayan, P. M. Super-Compressible Foamlike Carbon Nanotube Films. *Science* **2005**, *310*, 1307–1310.